Using Linear Spectral Unmixing for Subpixel Mapping of Hyperspectral Imagery: A Quantitative Assessment

Xiong Xu, Xiaohua Tong, Antonio Plaza, *Fellow, IEEE*, Yanfei Zhong, *Senior Member, IEEE*, Huan Xie, and Liangpei Zhang, *Senior Member, IEEE*

***Abstract*—Subpixel mapping techniques have been widely utilized to determine the spatial distribution of the different land-cover classes in mixed pixels at a subpixel scale by converting low-resolution fractional abundance maps (estimated by a linear mixture model) into a finer classification map. Over the past decades, many subpixel mapping algorithms have been proposed to tackle this problem. It has been obvious that the utilized abundance map has a strong impact on the subsequent subpixel mapping procedure. However, limited attention has been given to the impact of the different aspects in the spectral unmixing model on the subpixel mapping performance. In this paper, a detailed quantitative assessment of different aspects in linear spectral mixture analysis, such as the criteria used to determine the types of pixels, the abundance sum-to-one constraint in the unmixing, and the accuracy of the utilized abundance maps, is investigated. This is accomplished by designing an experimental procedure with replaceable components. A total of six hyperspectral images (four synthetic and two real) were utilized in our experiments. By investigating these critical issues, we can further improve the performance of subpixel mapping techniques.**

***Index Terms*—Hyperspectral imaging, spectral unmixing (SU), subpixel mapping.**

I. Introduction

MIXED pixels are often found in hyperspectral images, especially in those with low spatial resolution. In these images, a single pixel may comprise two or more different land-cover classes [1], [2]. To address this issue, soft classification and spectral unmixing (SU) techniques have been commonly used to quantitatively estimate the proportion of each pure spectral constituent (endmember) in the mixed pixel by establishing the relationship between the measured spectra of the mixed pixel and the corresponding representative spectra of the land-cover classes [3]. The linear spectral mixture model (LSMM), which is our focus in this contribution, has been one of the most widely used approaches for this purpose owing to its simplicity and effectiveness in dealing with the mixed pixel problem [1]. By assuming that the observed spectra of each pixel can be expressed in the form of a linear combination of endmembers, the LSMM can generate the corresponding weights of the different endmembers, which are the so-called abundance fractions [4]. The obtained abundance map can indicate the quantitative proportions of the land-cover classes in each pixel, whereas the spatial distribution of each endmember in the mixed pixel still remains unknown.

Subpixel mapping, which in most cases can be regarded as a subsequent procedure to SU, aims to arrange the spatial location of possible classes inside each mixed pixel given the obtained abundance map [5], [6]. By dividing the pixels into numerous smaller subpixels and allocating each subpixel to a certain class, subpixel mapping techniques can convert the low-resolution (LR) abundance map into a finer classification result given the criteria of abundance constraints and spatial dependence, which is inspired by Tobler's first law [7].

The spatial dependence refers to the tendency for spatially close observations to be more alike than distant observations [5]. Based on this assumption, much effort has been devoted to the development of subpixel mapping techniques, and most of these techniques attempt to retrieve a finer classification result based on the given abundance map [8], which is commonly obtained by the use of an LSMM technique [9]. Other soft classification methods have also been utilized to generate the abundance result, such as the maximum likelihood classifier [10], [11] and the fuzzy c-means method [12], [13]. However, only the LSMM will be considered in this paper.

Many algorithms have been proposed to convert the abundance map into the subpixel mapping result, such as the pixel-swapping algorithm [14]–[16], the Hopfield neural network [17], [18], the spatial attraction model (AM)

Manuscript received June 19, 2016; revised September 12, 2016; accepted October 23, 2016. Date of publication November 30, 2016; date of current version March 22, 2017. This work was supported in part by China Postdoctoral Science Foundation under Grant 2014M560353 and Grant 2015T80450, in part by the National Natural Science Foundation of China under Grant 41401398, Grant 41325005, Grant 41201426, Grant 41171352, and Grant 41171327, in part by the Fund of Shanghai Outstanding Academic Leaders Program under Grant 12XD1404900, and in part by Kwang-Hua Foundation of College of Civil Engineering, Tongji University. *(Corresponding author: Xiaohua Tong.)*

X. Xu is with the College of Surveying and Geo-Informatics, Tongji University, Shanghai 200092, China, and also with the Hyperspectral Computing Laboratory, Department of Technology of Computers and Communications, Escuela Politecnica, University of Exremadura, Cáceres 10003, Spain (e-mail: xvxiong@tongji.edu.cn).

X. Tong and H. Xie are with the College of Surveying and Geo-Informatics, Tongji University, Shanghai 200092, China (e-mail: xhtong@tongji.edu.cn; huanxie@tongji.edu.cn).

A. Plaza is with the Hyperspectral Computing Laboratory, Department of Technology of Computers and Communications, Escuela Politecnica, University of Exremadura, Cáceres 10003, Spain (e-mail: aplaza@unex.es).

Y. Zhong and L. Zhang are with the State Key Laboratory of Information Engineering in Surveying, Mapping and Remote Sensing, Wuhan University, Wuhan 430079, China (e-mail: zhongyanfei@whu.edu.cn; zlp62@whu.edu.cn).

Color versions of one or more of the figures in this paper are available online at http://ieeexplore.ieee.org

Digital Object Identifier 10.1109/JSTARS.2016.2624560

[19]–[21], genetic algorithms [22]–[24], multiagent systems [25], maximum *a posteriori*-based techniques [26]–[28], and differential evolution [29]. Furthermore, subpixel mapping techniques have been widely applied in various fields, including land-cover mapping [30], [31], target extraction [32]–[34], waterline mapping [35], [36], change detection [37], [38], and flood/wetland inundation [24], [39].

However, very few studies have considered the impact of the different aspects involved in the SU process and/or the generation of the most suitable abundance map for the subsequent subpixel mapping procedure. We believe that it is crucial to address these issues owing to the fact that the generated abundance map is, in most cases, the driving component for the subpixel mapping process. By investigating these critical issues, it may be possible to further improve the performance of subpixel mapping techniques. A number of experiments were therefore designed in this study to investigate the impact of the different aspects in the LSMM on the subsequent subpixel mapping procedure. Specifically, we intend attempt to give some recommendations on the best practice regarding the utilization of SU and subpixel mapping algorithms in different applications.

Three aspects were considered in our experimental analysis. First, as subpixel mapping aims to tackle mixed pixels, the determination of mixed pixels during the SU procedure is crucial. Second, whether or not it is essential to impose the abundance sum-to-one constraint (ASC) on the generated abundance map is still controversial [40], [41]. The impact of the incorporation of the ASC on the subpixel mapping result needs to be carefully studied. Finally, traditional subpixel mapping algorithms do not pay specific attention to the generation of the utilized abundance map, and it is commonly believed that the generation of an abundance map with higher accuracy can result in a better subpixel mapping result.

Based on these issues, this paper presents an exhaustive quantitative analysis on the widely used LSMM to evaluate the effects of different choices in its configuration on the subsequent subpixel mapping procedure. Specifically, the three aforementioned issues were taken into consideration in our experiments, conducted with six different hyperspectral datasets comprising both simulated and real images. Based on our experimental study, the impact of the different aspects in the LSMM on the subpixel mapping output is extensively discussed and some relevant conclusions are drawn.

The remainder of this paper is organized as follows. Section II provides a detailed description of the LSMM and the related aspects; the utilized experimental datasets are also described. Section III gives a detailed analysis and discussion of the obtained results. Section IV concludes this paper with some remarks and hints at plausible future research lines.

II. Method Materials and Methods

A. Experimental Design

As this paper aims to investigate the impact of the different factors in the LSMM on subpixel mapping, it is important to review the literature related to subpixel mapping, and to discuss the most appropriate design for the experiments in this paper. In general, there are three different approaches to designing subpixel mapping techniques [8]. In the early studies, to reduce the uncertainty in the subpixel mapping and make it easier to compare different algorithms, the utilized abundance map was always generated by degrading a high-resolution (HR) classification map, which was generally obtained by classifying a hyperspectral image, and applying an averaging filter, given a resize factor [8], [14]. In this way, the original HR classification map can be used as a reference image to evaluate the subpixel mapping method, and it is generally assumed that the utilized abundance map is unbiased so that the comparison is solely affected by errors introduced in the subpixel mapping process.

Furthermore, another approach consists of generating an LR hyperspectral image by degrading the available HR hyperspectral image with an averaging filter [42]. An SU technique is first used to obtain the abundance map from this LR hyperspectral image, and the subsequent subpixel mapping methods are then applied. Similarly, the classification result obtained by classifying the HR hyperspectral image can be used as a reference ground truth to evaluate the subpixel mapping results. In this way, except from the subpixel mapping model errors, the errors in the abundance map and the HR reference classification are also taken into consideration in the final performance evaluation. The two aforementioned approaches to generating synthetic images for subpixel mapping purposes can be referred to as "nonunmixing-based synthetic experiments" and "unmixing-based synthetic experiments."

Although synthetic experiments can illustrate the differences in subpixel mapping methods to some extent, real experiments are still essential to evaluate the application of subpixel mapping in practice. For real experiments, two images which cover the same area—an LR hyperspectral image and a finer reference one—are commonly acquired, preferably at the same time. Image registration is then performed and a suitable scale factor is determined. A final result can be then generated from the LR hyperspectral image after applying SU and subpixel mapping procedures, and the reference classification map is obtained after classifying the HR reference image. Therefore, the error of registration is further involved in the real experiment in addition to similar error sources with the unmixing-based synthetic experiment.

Fig. 1 summarizes the three different approaches to synthetic and real experiments, which are represented by different colored arrows. The black arrows denote the general procedure, while the light blue, purple, and red arrows indicate the nonunmixing/unmixing-based synthetic and real experiments, respectively.

B. Aspects in the LSMM

Given a hyperspectral dataset with *L* bands and *K* endmembers, the LSMM for the imagery with *m* rows and *n* columns ($mn = m * n$ pixels) can be represented as follows:

$$\mathbf{y} = \mathbf{S}\alpha + \mathbf{r} \tag{1}$$

where $\mathbf{y} \in \Re^{L \times mn}$ is the LR hyperspectral image with *L* bands and *mn* pixels, $\mathbf{S} = \{\mathbf{s}_1, \mathbf{s}_2 \cdots \mathbf{s}_K\} \in \Re^{L \times K}$ is the collected

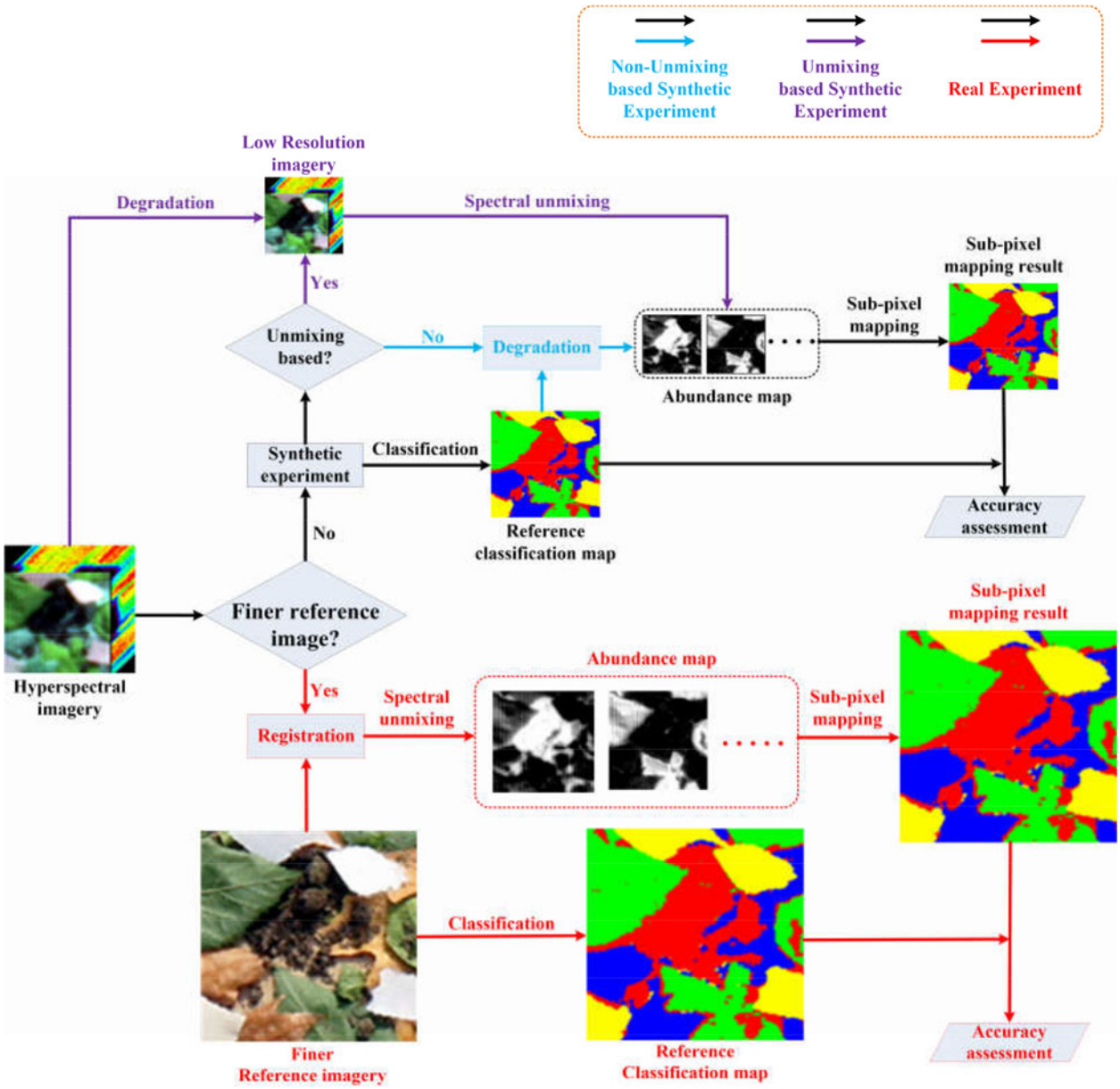

Fig. 1. Three different approaches to synthetic and real experiments.

spectral signatures of the K endmembers obtained manually or automatically, $\alpha \in \Re^{K\times mn}$ is the abundance map denoting the fraction values of the different endmembers, and $\mathbf{r} \in \Re^{L\times mn}$ is considered to be noise.

Owing to the physical meaning of the abundance map, two constraints are generally imposed. One is the abundance nonnegative constraint and the other is the previously mentioned ASC, illustrated in

$$\text{ANC}: \alpha_{k,i} \geq 0 \qquad \text{ASC}: \sum_{k=1}^{K} \alpha_{k,i} = 1 \tag{2}$$

where $\alpha_{k,i}$ denotes the fraction value of endmember k in pixel i.

Two tasks are generally involved in the LSMM. One is to determine if the target pixel is mixed or pure, and the other one is to calculate the proportions of the different classes in the mixed pixels. As the subpixel mapping operation is only conducted on the identified mixed pixels, the two aspects can have different implications, and therefore, need to be analyzed separately. As the utilization of the ASC in SU has been prone to some criticism [40], [41], it is also necessary to discuss the applicability of the ASC for the subsequent subpixel mapping procedure. In addition, the hypothesis that an abundance map with a higher accuracy can guarantee a better subpixel mapping result is also taken into consideration in this paper.

Therefore, three different factors in the LSMM are investigated in this paper to evaluate their impact on the subsequent subpixel mapping result: 1) the determination of the pixel type; 2) the utilization of the ASC; and 3) the impact of abundance map accuracy. To clearly describe the different

TABLE I
LIST OF SYMBOLS AND ABBREVIATIONS

Terms	Definition
SVM_{PD}	The SVM method is used for the PD to generate the probability map
$NCLS_{PD}$	The NCLS method is used for the PD
$FCLS_{PD}$	The FCLS method is used for the PD
$\mathbf{P}(*)$	The probability map which denotes the probabilities of pixels to belong different classes with certain PD method (SVM_{PD}, $NCLS_{PD}$ or $FCLS_{PD}$)
$p_{k,i}(*)$	The probability of pixel *i* belonging to class *k* in the probability map $\mathbf{P}(*)$.
T_S	The threshold to determine if a pixel is mixed for $\mathbf{P}(SVM_{PD})$
T_N	The threshold to determine if a pixel is mixed for $\mathbf{P}(NCLS_{PD})$
T_F	The threshold to determine if a pixel is mixed for $\mathbf{P}(FCLS_{PD})$
$NCLS_{SU}$	The NCLS method is used to generate abundance fractions for mixed pixels
$FCLS_{SU}$	The FCLS method is used to generate abundance fractions for mixed pixels

aspects in the LSMM, the notations and definitions are first described in Table I.

Our experimental assessments have been conducted as follows. First, three different methods were utilized to estimate the probability map $\mathbf{P}$ which was used to determine the nature of the pixel (mixed or pure): the support vector machine (SVM) [43], the nonnegativity constrained least squares (NCLS), and fully constrained least squares (FCLS) [44]. Accordingly, different parameters were also used as the thresholds, denoted as T_S, T_N, and T_F for the SVM_{PD}, $NCLS_{PD}$, and $FCLS_{PD}$ probability maps, respectively. The criteria for a certain pixel *i* in the different probability maps are given in (3) to determine if pixel *i* is mixed:

$$\begin{cases} p_{\max,i}(SVM_{PD}) < T_S, \\ p_{\max,i}(NCLS_{PD}) < 1 - T_N \\ \text{or} \quad p_{\text{sum},i}(NCLS_{PD}) - p_{\max,i}(NCLS_{PD}) > T_N, \\ p_{\max,i}(FCLS_{PD}) < 1 - T_F \end{cases} \tag{3}$$

where $p_{\max,i}(SVM_{PD}) = \max(p_{k,i}(SVM_{PD}))$ and $p_{\text{sum},i}(SVM_{PD}) = \sum_{k=1}^{K} p_{k,i}(SVM_{PD})$, while $p_{k,i}(SVM_{PD})$ is the probability of pixel *i* belonging to class *k* in the SVM-based probability map. In addition, one more criterion is utilized for NCLS considering that $p_{\text{sum},i}(NCLS_{PD})$ can be higher than one.

For those pixels which are determined as pure, a certain class label is assigned and they will not be unmixed by the subsequent unmixing procedure. After that, NCLS and FCLS were then used again to generate the fractional values for each class in the rest of the identified mixed pixels, denoted as $NCLS_{SU}$ and $FCLS_{SU}$. In this way, abundance maps with different combinations of pixel type determination (PD) and SU methods could be obtained.

Given the fact that only one certain class label can be assigned to each pixel in the classification map, the so-called label sum-to-constant constraint (LSC), which gives $\sum_{k=1}^{K} NS_i^k = S * S$, is defined as the constraint for the generated subpixel mapping result where the NS_i^k is the number of subpixels belonging to class *k* in the mixed pixel *i*.

In general, to guarantee the LSC in the final subpixel mapping result, only abundance maps which satisfy the ASC can be processed by most subpixel mapping methods which either strictly internalize the ASC [19], [20] or are iterative methods in which an initial classification map is essential [29]. Therefore, two typical subpixel mapping methods—the subpixel/pixel AM [19] and the class determination (CD) strategy [21]—were employed to convert the abundance maps into the final subpixel mapping results. Specifically, the CD method can be further imposed on abundance maps generated by the NCLS unmixing method, while the AM method can only be used on FCLS-based abundance maps. The workflow of the experiments is illustrated in Fig. 2.

C. Datasets

Six datasets (four synthetic remotely sensed images and two real hyperspectral images) were utilized to evaluate the impact of the three previously mentioned factors in the LSMM. Specifically, the endmember set utilized in the LSMM is selected from the image manually based on extensive prior knowledge. This allows us to substantiate our proposed approach independently by the performance of different endmember selection algorithms.

1) Synthetic Dataset 1: Washington DC Hyperspectral Digital Imagery Collection Experiment (HYDICE) Image: The first image was generated from a part of the HYDICE airborne hyperspectral dataset collected over the Washington DC Mall. A total of 167 bands [45] were used, comprising 300 lines and 200 columns. The scale factor was 4, and the generated LR hyperspectral image (75∗50 pixels) is shown in Fig. 3(a). Fig. 3(b) shows the reference image classified by the SVM method for the HR image, which we use here as the ground-truth data. The image comprises four main classes: water, grass, tree, and roads.

2) Synthetic Dataset 2: Xiaqiao PHI Image: The second synthetic remote sensing image was collected with an airborne imaging spectrometer (PHI) from the Xiaqiao test site in China. A total of 80 bands of the PHI image (160 × 160 pixels) were utilized, with a spectral range of 440–854 nm. The scale factor was again set as 4. Fig. 3(c) shows the LR hyperspectral image cube. Fig. 3(d) shows the reference classification map obtained by SVM in which four major land-cover classes can be distinguished: roads, water, corn, and vegetables.

3) Synthetic Dataset 3: Flightline C1 (FLC1) Image: The third image was an aerial image of different crop types and land use, (band number 12) by an optical mechanical line scanner referred to as the University of Michigan M-7 system. The image used in this experiment (which is referred to as FLC1) was collected on June 28, 1966 [46], and was taken over the southern part of Tippecanoe County of Indiana. The size in pixels of the image is 80 × 160 pixels, and the LR image was generated using a scale factor of 4, as shown in Fig. 3(e). A classification result was then obtained for FLC1 by classifying the original HR image with the commercial

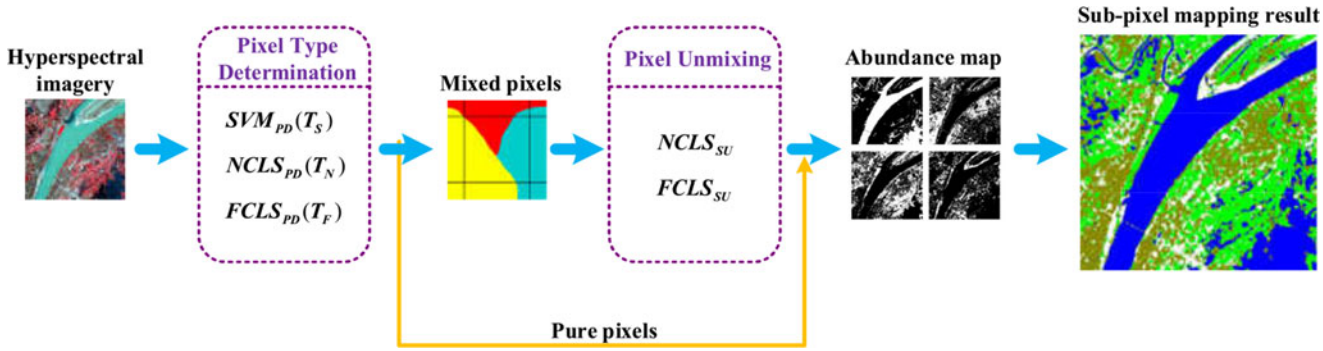

Fig. 2. Workflow of the experiments.

eCognition software. A total of eight land-cover classes can be distinguished in Fig. 3(f).

4) Synthetic Dataset 4: Pavia Center Dataset: Another hyperspectral dataset used in this study was collected in the framework of the HySens project, managed by DLR (the German Aerospace Centre) and sponsored by the European Union. This experimental image is a subset of the image of Pavia city center, which was acquired by the reflective optics system imaging spectrometer (ROSIS) sensor during a flight campaign over Pavia, northern Italy, on 8 July, 2002. A total of 97 bands of the ROSIS image (488*1096 pixels) were utilized after some noisy bands were excluded. The scale factor was set as 4. A false-color image consisting of bands 84, 48, and 11 as the R, G, and B bands is illustrated in Fig. 3(g). Fig. 3(h) shows the ground truth to evaluate the classification results. The number of classes in the hyperspectral image was 9: water, tree, meadow, brick, bare soil, asphalt, bitumen, tile, and shadow.

5) Real Dataset 1: Nuance 1 Dataset: The real-data experiments were conducted using two pairs of low and high spatial resolution images collected simultaneously over the same area. The two LR hyperspectral images were both collected using a Nuance NIR imaging spectrometer, and the acquired images consisted of 46 bands, collected in the spectral range of 650–1100 nm, and with a 10 nm spectral sampling interval. Meanwhile, the two HR color images were obtained by a digital camera for the same areas as the LR images. After the LR and HR images were obtained, the ENVI software was introduced to accomplish the registration. For the Nuance 1 dataset, the size of the LR image was 50*50 pixels and the HR image was 150*150 pixels, so the scale factor was exactly 3. The LR hyperspectral image and the HR color image are shown in Fig. 4(a) and (b), respectively. A reference classification map was obtained using the SVM technique on the HR image, as shown in Fig. 4(c), in which three major land-cover classes can be distinguished: withered vegetation, fresh vegetation, and black paper, which was used as the background.

6) Real Dataset 2: Nuance 2 Dataset: The second Nuance dataset, as shown as Fig. 4(d), contained 80*80 pixels, and the size of the corresponding HR color image was 160*160 pixels, given that the scale factor was 2. The reference classification map was again obtained by classifying the HR image [as shown in Fig. 4(e)] with the SVM method. Four major land-cover classes can be distinguished in Fig. 4(f): soil, fresh vegetation, withered vegetation, and white paper.

III. Experiments and Discussion

Given the six images described in the previous section, the subpixel mapping results generated with the workflows described above were obtained. As NCLS and FCLS were both utilized in the PD together with different SU procedures, different notations are utilized to denote them. For example, $NCLS_{PD}$ means that the NCLS method was used to determine the type of pixels. Therefore, six combinations ($SVM_{PD} + NCLS_{SU}$; $SVM_{PD} + FCLS_{SU}$; $NCLS_{PD} + NCLS_{SU}$; $NCLS_{PD} + FCLS_{SU}$; $FCLS_{PD} + NCLS_{SU}$; $FCLS_{PD} + FCLS_{SU}$) were designed to obtain different abundance maps, and two different subpixel mapping methods (AM and CD) were introduced, in which three factors were involved: 1) the PD method; 2) the integration of the ASC in the abundance map; and 3) the impact of abundance map accuracy on the final subpixel mapping assessment. In addition, for the three PD methods, different thresholds (T_S, T_N, and T_F) were also tested. In experiments, T_S was varied from 0.4 to 1 while T_N and T_F were increased from 0 to 0.6, both with an interval of 0.05. Specifically, if $T_S = 1$, $T_N = 0$, and $T_F = 0$, the utilized PD operators were not activated as all the pixels were then assumed to be mixed pixels.

Finally, to accomplish the task of accuracy assessment, the root-mean-square error (RMSE) index was utilized to compare the generated abundance results with the reference abundance map that was obtained by degrading the reference classification map [47]. At the same time, the accuracy assessment of the subpixel mapping was undertaken by the use of the classification overall accuracy and Kappa coefficient [48].

A. Impact of the PD Operator

Three different PD methods (SVM_{PD}, $NCLS_{PD}$, and $FCLS_{PD}$) were evaluated, and for each PD method, different thresholds were tested. Two SU methods ($NCLS_{SU}$ and $FCLS_{SU}$) were employed to generate the abundance maps. Moreover, to demonstrate the impact of the PD procedure, the two SU methods were also used to generate the abundance map without the previous PD procedure, and the final results were compared with the PD method-based subpixel mapping results. For convenience, this is termed the "non-PD" method.

1) Comparison of the Different PD Methods: Two subpixel mapping methods (AM and CD) were utilized to obtain the subpixel mapping results for the $NCLS_{SU}$- and $FCLS_{SU}$-based

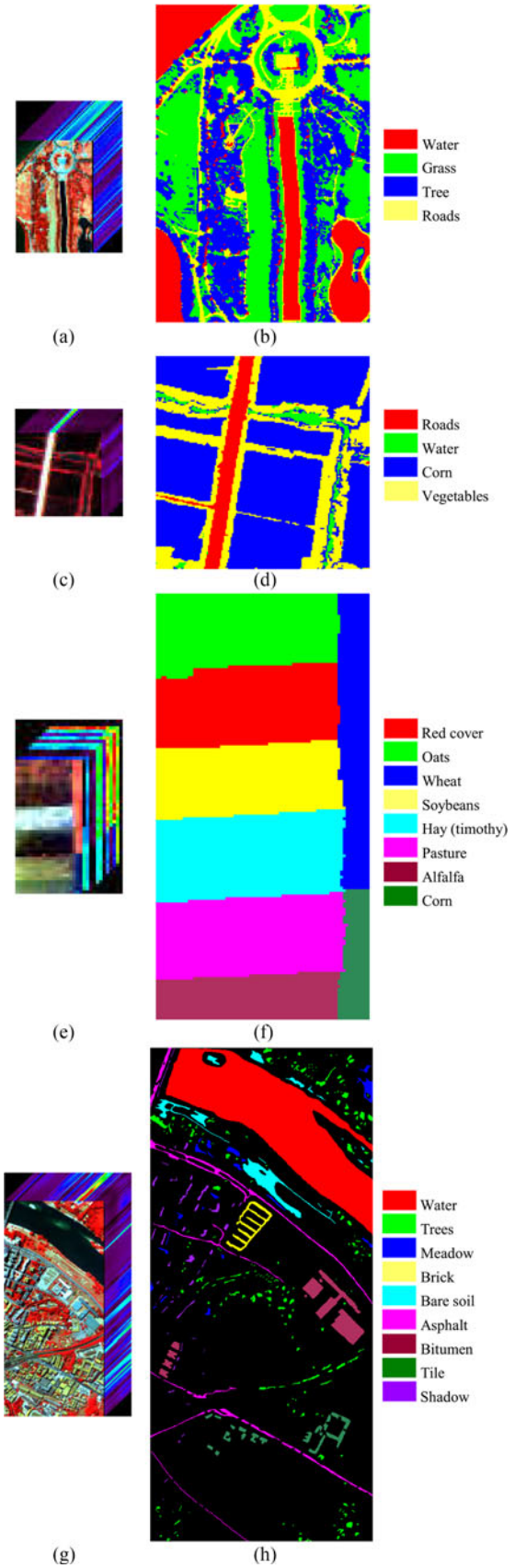

Fig. 3. Four synthetic remotely sensed datasets: (a) and (b) Washington DC. (c) and (d) Xiaqiao. (e) and (f) FLC1. (g) and (h) Pavia center.

abundance maps. For each dataset, the subpixel mapping results with the best accuracies from the three PD methods and the non-PD result are shown in Fig. 5. Here, it is clear that the PD procedures have a great impact on the final subpixel mapping result. For all the datasets, the PD procedures give a great improvement by deciding if a pixel needs to be unmixed or identified as a pure pixel beforehand. This is because many pure pixels may be misclassified as mixed pixels in the abundance map with the non-PD procedure, owing to the endmember variability in real circumstances. However, an additional PD operator can give a certain degree of relaxation, as (3) shows, so that the misclassification of mixed pixels can be alleviated and a better subpixel mapping result can be obtained.

Among the three different PD methods, it is clear that SVM_{PD} exhibits the best performance for all the datasets. This is because the SVM_{PD} method utilizes a set of training samples for each class, in which the endmember variability is considered to determine if a given pixel is mixed. Meanwhile, for the other two methods, only one representative spectrum of each class is used for the linear SU procedure.

In general, the PD procedure has the potential to improve the performance of the final subpixel mapping result by giving a degree of abundance relaxation so that the endmember variability can be taken into consideration. The SVM_{PD} method in particular can generate a better result in all cases by utilizing a set of labeled samples.

2) Comparison of the Impact of Different Thresholds in the PD Methods: The impact of the different thresholds on the performance of the PD methods was also investigated. In addition to each PD method, the $FCLS_{SU}$ and AM methods were utilized to generate the subpixel mapping results. The three PD methods were employed for this comparison, as shown in Fig. 6, where it can be seen that it is important to select a proper threshold for each PD method. It is not surprising that the curves of the images are not exactly the same. The optimal threshold setting for each dataset is different, and the peaks of the curves can only be observed for the DC and Xiaqiao images, while the accuracies of the other datasets increase or decrease monotonically. This phenomenon may be related to the spatial distribution of the different land-cover classes in the images, and it can be seen from Fig. 3 that more heterogeneous areas can be distinguished in the DC and Xiaqiao images. This suggests that a moderate parameter setting may be suitable for images with complex spatial distributions, but for those more homogeneous datasets, the optimal threshold is difficult to determine. As (3) indicates, a smaller value of T_S and a greater value of T_N or T_F imply that vague pixels are more likely to be classified as pure pixels, and we can therefore hypothesize that subpixel mapping can benefit from avoiding excessive mixed PD by the use of proper thresholds. However, how to determine the optimal thresholds for the different PD methods still needs to be further studied.

B. Impact of ASC Integration

Two different SU methods—$NCLS_{SU}$ and $FCLS_{SU}$—were utilized to evaluate the impact of the ASC on the final subpixel mapping performance. To avoid the interference of the

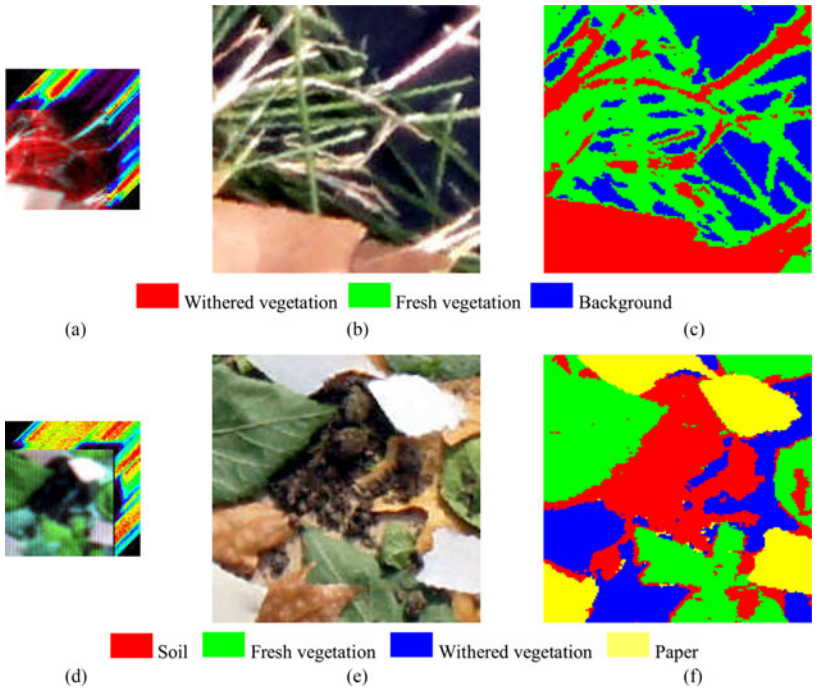

Fig. 4. Two real hyperspectral datasets: (a)–(c) Nuance 1 dataset. (d)–(f) Nuance 2 dataset.

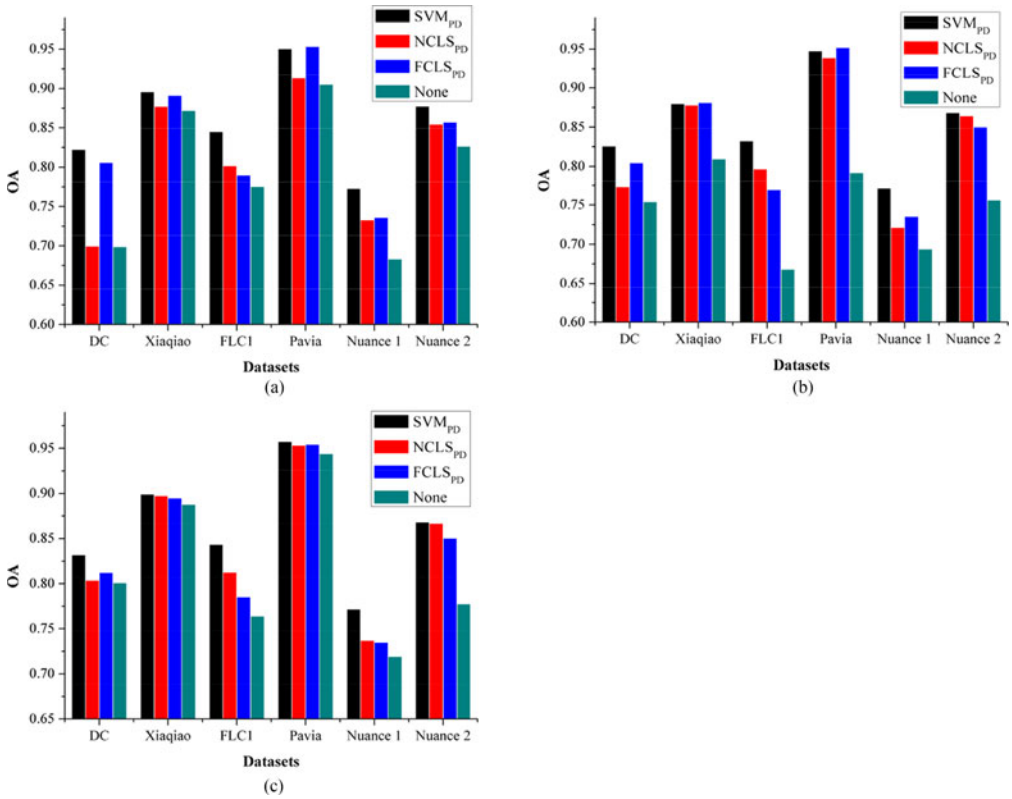

Fig. 5. Comparison of the three PD methods and the non-PD operator with different datasets: (a) $NCLS_{SU} + CD$, (b) $FCLS_{SU} + AM$, and (c) $FCLS_{SU} + CD$.

PD method, the PD procedure was not involved. As mentioned before, the abundance map generated by $NCLS_{SU}$ can only be handled by the CD method, so the CD method was utilized for both abundance maps with the $NCLS_{SU}$ and $FCLS_{SU}$ methods to avoid the disturbance from the different subpixel mapping methods. The subpixel mapping results for all the datasets are given for comparison in Fig. 8.

As can be seen in Fig. 7, it is $FCLS_{SU}$ which generates better results than the $NCLS_{PD}$-based results for most datasets, except for FLC1 and Nuance 2. For the FLC1 image, the

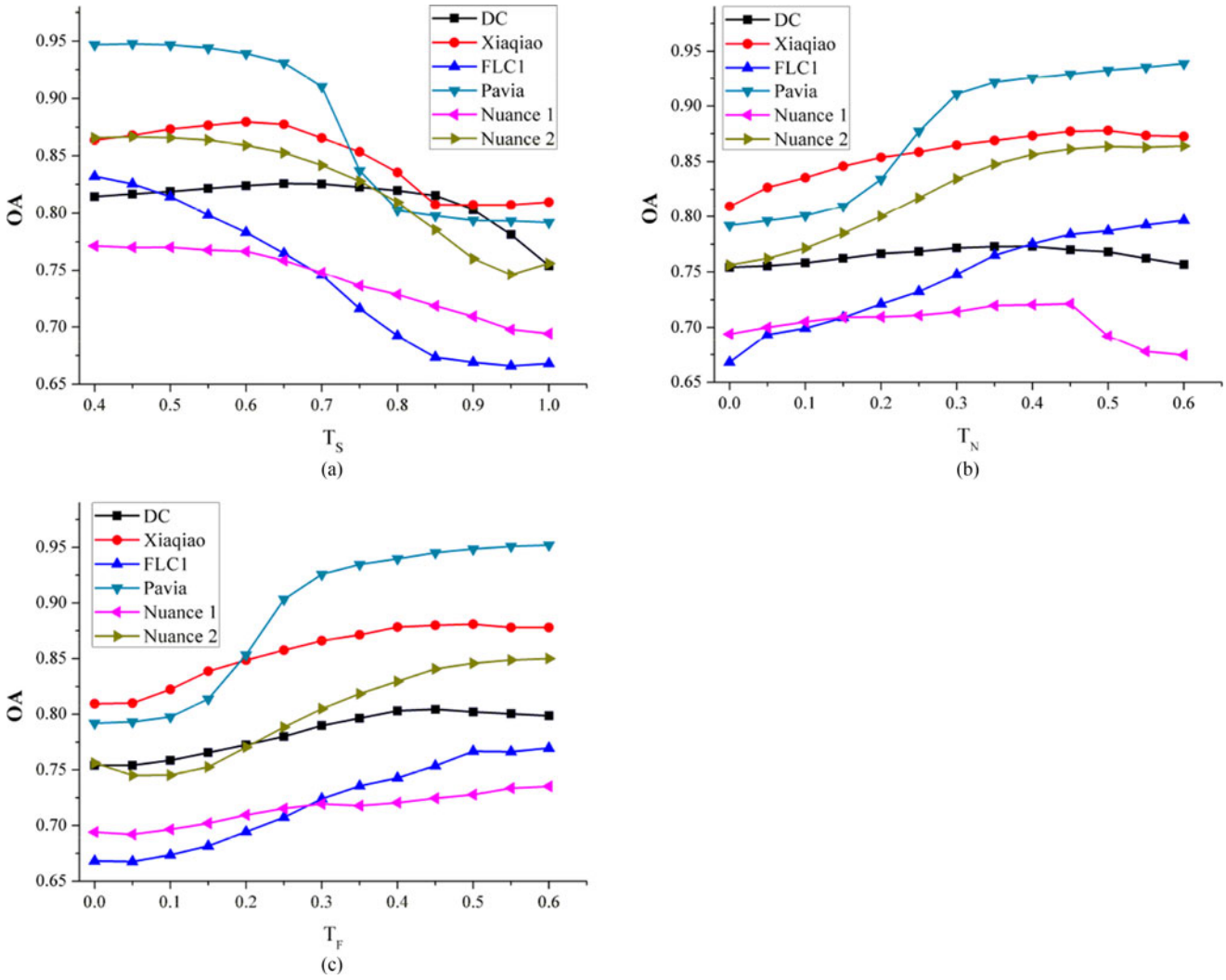

Fig. 6. Accuracy assessment of the different thresholds in the three PD methods: (a) $SVM_{PD} + FCLS_{SU} + AM$, (b) $NCLS_{PD} + FCLS_{SU} + AM$, and (c) $FCLS_{PD} + FCLS_{SU} + AM$.

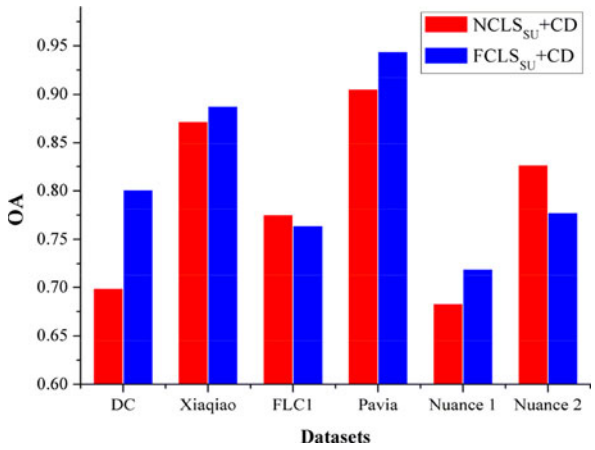

Fig. 7. Impact of the incorporation of the ASC in the abundance maps of all the datasets.

difference between the $NCLS_{PD}$- and $FCLS_{SU}$-based subpixel mapping results is subtle, and it is more apparent for Nuance 2. It is assumed that there is a relationship between the performance of the two methods and the scale factor. However, more datasets are needed to study the possible connection.

In general, it is apparent that the integration of the ASC has a great impact on the final result, and owing to the outstanding performance of $FCLS_{SU}$ in the three hyperspectral experiments, abundance maps incorporating the ASC have the potential to improve the subpixel mapping accuracy.

C. Impact of Abundance Accuracy

It is generally believed that an abundance map with a higher accuracy can generate a better subpixel mapping result. Experiments were, therefore, conducted to test this deduction. The SVM_{PD} method with different thresholds and $FCLS_{SU}$ were introduced to generate a set of abundance maps for each dataset. Furthermore, the AM method was used to generate the corresponding subpixel mapping results. The accuracy of the abundance maps was quantified with RMSE where the reference abundance maps were produced by degrading the reference classification maps.

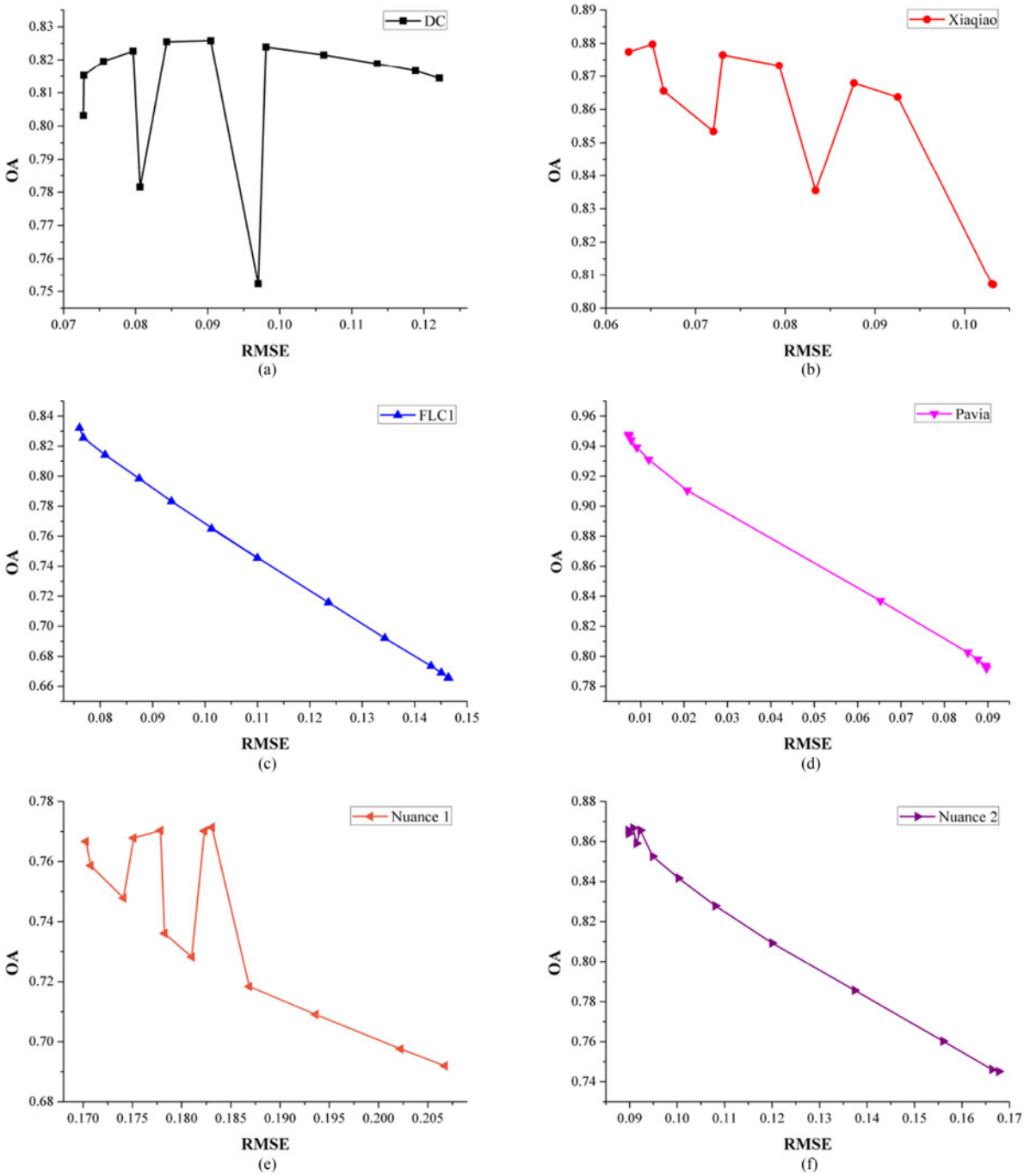

Fig. 8. Impact of the abundance accuracy on the subpixel mapping result ($SVM_{PD} + FCLS_{SU} + AM$) for all datasets. (a) Washington DC. (b) Xiaqiao. (c) FLC1. (d) Pavia center. (e) Nuance 1. (f) Nuance 2.

Fig. 8 shows the relationship between the accuracy of the estimated abundance maps and the corresponding subpixel mapping results for all six datasets. Specifically, the abundance map accuracy was varied from 0.4 to 1 with an interval of 0.05, and the results were sorted in ascending order in terms of RMSE values. Given the hypothesis that the accuracies of the subpixel mapping results increase with better abundance maps, the curves in Fig. 8 should decrease monotonically. However, it can be observed in Fig. 8 that this assumption does not hold in most of the datasets, except for FLC1 and Pavia center, and many anomalies can be observed.

For the anomalous results, a possible explanation is that only quantitative errors can be observed in the abundance maps while, for the subpixel mapping results, spatial displacement is also taken into consideration. If the subpixel mapping algorithm cannot work effectively, the consistency between the abundance maps and the subpixel mapping results may be broken, and an abundance map with a lower quality could generate a better result. In most cases, an accurate abundance map can ensure the quality of the final subpixel mapping result; however, the utilized subpixel mapping algorithm is also important to make the best possible use of this abundance map.

IV. Conclusion and Future Research Lines

In this paper, we have provided a detailed investigation of different factors affecting the SU process and their implication on subsequent subpixel mapping operations. The aim was to search for strategies to further improve the performance of subpixel mapping, which is commonly conducted based on abundance maps generated with an SU technique. Three main aspects, the PD, the integration of the ASC in the abundance map, and the impact of abundance map accuracy, were investigated to assess their impact through experiments with three different PD methods (SVM_{PD}, $NCLS_{PD}$, and $FCLS_{PD}$) and two SU approaches ($NCLS_{SU}$ and $FCLS_{SU}$). The thresholds considered in the three PD methods were also extensively evaluated and two different subpixel mapping algorithms—an AM and a CD strategy—were used in conjunction with the $NCLS_{SU}$ and $FCLS_{SU}$-based abundance maps. The experiments were conducted using six datasets (four simulated and two real hyperspectral images). The experiments revealed interesting observations.

1) First, the PD operation, which is commonly internalized in most SU methods, has a great impact on the subsequent subpixel mapping procedure, in which only mixed pixels are processed. Among the three PD methods considered in this study, SVM_{PD} exhibited the best performance due to its consideration of endmember variability by employing a set of training samples. To generate the abundance map used for subpixel mapping, the SU method should be selected carefully by assessing its ability to deal with the mixed PD problem.
2) Second, $NCLS_{SU}$ and $FCLS_{SU}$ were tested as linear SU methods to investigate the need to incorporate the ASC in the generated abundance map. According to our comparisons, it is difficult to give a definite conclusion for all datasets. However, it could still be seen that $FCLS_{PD}$ gave better results for most of the datasets. It is hypothesized here that an abundance map incorporating the ASC has the potential to improve the subpixel mapping result. However, the relationship between the ASC and datasets with different spatial distributions and scale factors needs to be further investigated.
3) Last but not least, when it comes to assessing the correlation between the abundance map accuracy and the subpixel mapping result, it is apparent that a positive relationship can be observed in some cases. However, many exceptions suggest that the subpixel mapping method needs to be selected properly to maintain this relationship. In addition, the traditional indexes used to evaluate subpixel mapping results cannot reveal the subpixel spatial distribution within mixed pixels and, therefore, spatial evaluation indicators should be used to assess the subpixel mapping performance. In our future work, more factors will be tested in the subpixel mapping procedure, such as endmember variability. Moreover, validation with additional datasets and different algorithms will also be studied in future developments.

Acknowledgment

The authors greatly appreciate the valuable comments and suggestions of the anonymous reviewers for improving the paper.

References

[1] J. M. Bioucas-Dias, A. Plaza, G. Camps-Valls, P. Scheunders, N. Nasrabadi, and J. Chanussot, "Hyperspectral remote sensing data analysis and future challenges," *IEEE Geosci. Remote Sens. Mag.*, vol. 1, no. 2, pp. 6–36, Jun. 2013.
[2] C.-I. Chang, *Hyperspectral Imaging: Spectral Detection and Classification*. New York, NY, USA: Plenum, 2003.
[3] J. M. Bioucas-Dias *et al.*, "Hyperspectral unmixing overview: Geometrical, statistical and sparse regression-based approaches," *IEEE J. Sel. Topics Appl. Earth Observ. Remote Sens.*, vol. 5, no. 2, pp. 354–379, Apr. 2012.
[4] C. Quintano, A. Fernández-Manso, Y. E. Shimabukuro, and G. Pereira, "Spectral unmixing," *Int. J. Remote Sens.*, vol. 33, pp. 5307–5340, 2012.
[5] P. M. Atkinson, "Mapping sub-pixel boundaries from remotely sensed images," in *Innovations in GIS IV*. London, U.K.: Taylor & Francis, 1997, ch. 12, pp. 166–180.
[6] P. M. Atkinson, "Issues of uncertainty in super-resolution mapping and the design of an inter-comparison study," in *Proc. 8th Int. Symp. Spatial Accuracy Assessment Natural Resources Environ. Sci.*, Shanghai, China, 2004, pp. 145–154.
[7] W. R. Tobler, "A computer movie simulating urban growth in the Detroit region," *Econ. Geography*, vol. 46, pp. 234–240, Jun. 1970.
[8] X. Xu, "Sub-pixel mapping theory considering spatial characteristic for remote sensing imagery," Ph.D. dissertation, State Key Lab. of Inf. Eng. Surveying, Mapping and Remote Sensing, Wuhan Univ., Wuhan, China, 2013.
[9] A. M. Muad, "Super-resolution mapping," Ph.D. dissertation, School of Geography, Univ. Nottingham, Nottingham, U.K., 2011.
[10] R. J. Samworth and M. Yuan, "Independent component analysis via nonparametric maximum likelihood estimation," *Ann. Statist.*, vol. 40, pp. 2973–3002, 2012.
[11] R. A. Schowengerdt, "On the estimation of spatial-spectral mixing with classifier likelihood functions," *Pattern Recognit. Lett.*, vol. 17, pp. 1379–1387, 1995.
[12] G. M. Foody, "Approaches for the production and evaluation of fuzzy land cover classifications from remotely-sensed data," *Int. J. Remote Sens.*, vol. 17, pp. 1317–1340, 1996.
[13] X. Li, F. Ling, and Y. Du, "Super-resolution mapping based on the supervised fuzzy c-means approach," *Remote Sens. Lett.*, vol. 3, pp. 501–510, 2012.
[14] P. M. Atkinson, "Sub-pixel target mapping from soft-classified, remotely sensed imagery," *Photogramm. Eng. Remote Sens.*, vol. 71, no. 7, pp. 839–846, Jul. 2005.
[15] Y. F. Su, G. M. Foody, A. M. Muad, and K. S. Cheng, "Combining pixel swapping and contouring methods to enhance super-resolution mapping," *IEEE J. Sel. Topics Appl. Earth Observ. Remote Sens.*, vol. 5, no. 5, pp. 1428–1437, Oct. 2012.
[16] C. Huang, Y. Chen, and J. Wu, "DEM-based modification of pixel-swapping algorithm for enhancing floodplain inundation mapping," *Int. J. Remote Sens.*, vol. 35, pp. 365–381, 2014.
[17] A. J. Tatem, H. G. Lewis, P. M. Atkinson, and M. S. Nixon, "Super-resolution target identification from remotely sensed images using a Hopfield neural network," *IEEE Trans. Geosci. Remote Sens.*, vol. 39, no. 4, pp. 781–796, Apr. 2001.
[18] X. Li, F. Ling, Y. Du, Q. Feng, and Y. Zhang, "A spatial-temporal Hopfield neural network approach for super-resolution land cover mapping with multi-temporal different resolution remotely sensed images," *ISPRS J. Photogramm. Remote Sens.*, vol. 93, pp. 76–87, 2014.
[19] K. C. Mertens, B. D. Baets, L. P. C. Verbeke, and R. R. D. Wulf, "A sub-pixel mapping algorithm based on sub-pixel/pixel spatial attraction models," *Int. J. Remote Sens.*, vol. 27, no. 15, pp. 3293–3310, Aug. 2006.
[20] X. Tong, X. Zhang, J. Shan, H. Xie, and M. Liu, "Attraction-repulsion model-based subpixel mapping of multi-/hyperspectral imagery," *IEEE Trans. Geosci. Remote Sens.*, vol. 51, no. 5, pp. 2799–2814, May 2013.
[21] X. Xu, Y. Zhong, and L. Zhang, "A sub-pixel mapping method based on an attraction model for multiple shifted remotely sensed images," *Neurocomputing*, vol. 134, pp. 79–91, 2014.

[22] K. C. Mertens, L. P. C. Verbeke, E. I. Ducheyne, and R. R. D. Wulf, "Using genetic algorithms in sub-pixel mapping," *Int. J. Remote Sens.*, vol. 24, no. 21, pp. 4241–4247, Nov. 2003.
[23] C. Zhao, W. Liu, Y. Wang, and X. Li, "Modified genetic algorithm-based sub-pixel mapping," *Optik*, vol. 125, pp. 6379–6383, 2014.
[24] L. Li, Y. Chen, T. Xu, R. Liu, K. Shi, and C. Huang, "Super-resolution mapping of wetland inundation from remote sensing imagery based on integration of back-propagation neural network and genetic algorithm," *Remote Sens. Environ.*, vol. 164, nos. 3/4, pp. 142–154, Jul. 2015.
[25] X. Xu, Y. Zhong, and L. Zhang, "Adaptive sub-pixel mapping based on a multi-agent system for remote sensing imagery," *IEEE Trans. Geosci. Remote Sens.*, vol. 52, no. 2, pp. 787–804, Feb. 2014.
[26] X. Xu, Y. Zhong, L. Zhang, and H. Zhang, "Sub-pixel mapping based on a MAP model with multiple shifted hyperspectral imagery," *IEEE J. Sel. Topics Appl. Earth Observ. Remote Sens.*, vol. 6, no. 2, pp. 580–593, Apr. 2013.
[27] Y. F. Zhong, Y. Y. Wu, L. P. Zhang, and X. Xu, "Adaptive MAP sub-pixel mapping model based on regularization curve for multiple shifted hyperspectral imagery," *ISPRS J. Photogramm. Remote Sens.*, vol. 96, pp. 134–148, 2014.
[28] Y. F. Zhong, Y. Y. Wu, X. Xu, and L. P. Zhang, "An adaptive subpixel mapping method based on map model and class determination strategy for hyperspectral remote sensing imagery," *IEEE Trans. Geosci. Remote Sens.*, vol. 53, no. 3, pp. 1411–1426, Mar. 2015.
[29] Y. Zhong and L. Zhang, "Remote sensing image sub-pixel mapping based on adaptive differential evolution," *IEEE Trans. Syst., Man, Cybern. B, Cybern.*, vol. 42, no. 5, pp. 1306–1329, Oct. 2012.
[30] A. J. Tatem, H. G. Lewis, P. M. Atkinson, and M. S. Nixon, "Increasing the spatial resolution of agricultural land cover maps using a Hopfield neural network," *Int. J. Geographical Inf. Sci.*, vol. 17, no. 7, pp. 647–672, Oct./Nov. 2003.
[31] Y. Ge, "Sub-pixel land-cover mapping with improved fraction images upon multiple-point simulation," *Int. J. Appl. Earth Observ. Geoinf.*, vol. 22, pp. 115–126, 2013.
[32] J. P. Ardila, V. A. Tolpekin, W. Bijker, and A. Stein, "Markov-random-field-based super-resolution mapping for identification of urban trees in VHR images," *ISPRS J. Photogramm. Remote Sens.*, vol. 66, pp. 762–775, 2011.
[33] Y. Shao and R. S. Lunetta, "Sub-pixel mapping of tree canopy, impervious surfaces, and cropland in the Laurentian Great Lakes Basin using MODIS time-series data," *IEEE J. Sel. Topics Appl. Earth Observ. Remote Sens.*, vol. 4, no. 2, pp. 336–347, Jun. 2011.
[34] M. W. Thornton, P. M. Atkinson, and D. A. Holland, "Sub-pixel mapping of rural land cover objects from fine spatial resolution satellite sensor imagery using super-resolution pixel swapping," *Int. J. Remote Sens.*, vol. 27, pp. 473–491, 2006.
[35] G. M. Foody, A. M. Muslim, and P. M. Atkinson, "Super-resolution mapping of the waterline from remotely sensed data," *Int. J. Remote Sens.*, vol. 26, pp. 5381–5392, 2005.
[36] A. M. Muad and G. M. Foody, "Super-resolution mapping of lakes from imagery with a coarse spatial and fine temporal resolution," *Int. J. Appl. Earth Observ. Geoinf.*, vol. 15, pp. 79–91, 2012.
[37] F. Ling, W. Li, Y. Du, and X. Li, "Land cover change mapping at the subpixel scale with different spatial-resolution remotely sensed imagery," *IEEE Geosci. Remote Sens. Lett.*, vol. 8, no. 1, pp. 182–186, Jan. 2011.
[38] Q. M. Wang, P. M. Atkinson, and W. Z. Shi, "Fast subpixel mapping algorithms for subpixel resolution change detection," *IEEE Trans. Geosci. Remote Sens.*, vol. 53, no. 4, pp. 1692–1706, Apr. 2015.
[39] L. Li, Y. Chen, X. Yu, R. Liu, and C. Huang, "Sub-pixel flood inundation mapping from multispectral remotely sensed images based on discrete particle swarm optimization," *ISPRS J. Photogramm. Remote Sens.*, vol. 101, pp. 10–21, 2015.
[40] I. Dópido, M. Zortea, A. Villa, A. Plaza, and P. Gamba, "Unmixing prior to supervised classification of remotely sensed hyperspectral images," *IEEE Geosci. Remote Sens. Lett.*, vol. 8, no. 4, pp. 760–764, Jul. 2011.
[41] I. Dópido, A. Villa, A. Plaza, and P. Gamba, "A quantitative and comparative assessment of unmixing-based feature extraction techniques for hyperspectral image classification," *IEEE J. Sel. Topics Appl. Earth Observ. Remote Sens.*, vol. 5, no. 2, pp. 421–435, Apr. 2012
[42] A. Ertürk, M. K. Güllü, D. Çesmeci, D. Gerçek, and S. Ertürk, "Spatial resolution enhancement of hyperspectral images using unmixing and binary particle swarm optimization," *IEEE Geosci. Remote Sens. Lett.*, vol. 11, no. 12, pp. 2100–2104, Dec. 2014.
[43] A. Villa, J. Chanussot, J. A. Benediktsson, and C. Jutten, "Spectral unmixing for the classification of hyperspectral images at a finer spatial resolution," *IEEE J. Sel. Topics Signal Process.*, vol. 5, no. 3, pp. 521–533, Jun. 2011.
[44] D. Heinz and C.-I Chang, "Fully constrained least squares linear spectral mixture analysis method for material quantification in hyperspectral imagery," *IEEE Trans. Geosci. Remote Sens.*, vol. 39, no. 3, pp. 529–545, Mar. 2001.
[45] D. Landgrebe, *Signal Theory Methods in Multispectral Remote Sensing*. Hoboken, NJ, USA: Wiley, 2003.
[46] R. M. Hoffer, "Computer-aided analysis of multispectral scanner data—The beginnings," in *Proc. Amer. Soc. Photogramm. Remote Sens. Annu. Conf. 2009*, Mar. 9–13, 2009.
[47] (2016). [Online]. Available: https://en.wikipedia.org/wiki/Root-mean-square_deviation.
[48] S. V. Stehman, "Selecting and interpreting measures of thematic classification accuracy," *Remote Sens. Environ.*, vol. 62, pp. 77–89, 1997.

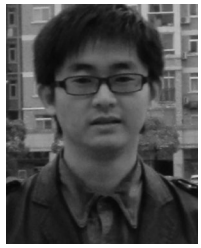

Xiong Xu received the B.Sc. degree in photogrammetry, in June 2008, and the Ph.D. degree in photogrammetry and remote sensing in June 2013, from Wuhan University, Wuhan, China.

He is currently a Research Assistant with the College of Surveying and Geoinformatics, Tongji University, China. His current research interests include multi- and hyperspectral image processing, artificial neural network, and pattern recognition.

Xiaohua Tong received the Ph.D. degree from Tongji University, China, in 1999.

He was a Postdoctoral Researcher in the State Key Laboratory of Information Engineering in Surveying, Mapping, and Remote Sensing, Wuhan University, China, between 2001 and 2003; a Research Fellow in The Hong Kong Polytechnic University in 2006, and a Visiting Scholar at the University of California, Santa Barbara, between 2008 and 2009. He is also a "Chang-Jiang Scholar" Chair Professor appointed by the Ministry of Education, China. His current research interests include remote sensing, GIS, trust in spatial data, image processing for high-resolution, and hyper-spectral images.

Dr. Tong is the Vice-Chair of the Commission on Spatial Data Quality of the International Cartographical Association, and the Co-Chair of the ISPRS working group (WG II/4) on Spatial Statistics and Uncertainty Modeling.

Antonio Plaza (M'05–SM'07–F'15) received the computer engineering degree and the M.Sc. and Ph.D. degrees in computer engineering from the University of Extremadura, Badajoz, Spain, in 1998, 2000, and 2002, respectively.

Dr. Plaza is a Fellow of IEEE "for contributions to hyperspectral data processing and parallel computing of Earth Observation data." He is an Associate Professor (with accreditation for Full Professor) in the Department of Technology of Computers and Communications, University of Extremadura, Badajoz, Spain, where he is the Head of the Hyperspectral Computing Laboratory (HyperComp). He was the Coordinator of the Hyperspectral Imaging Network, a European project with total funding of 2.8 MEuro (2007–2011). He has authored more than 500 publications, including more than 150 JCR journal papers (106 in IEEE journals), 22 book chapters, and more than 250 peer-reviewed conference proceeding papers (125 in IEEE conferences). He has guest edited seven special issues on JCR journals (three in IEEE journals). He has been the Chair for the IEEE Workshop on Hyperspectral Image and Signal Processing: Evolution in Remote Sensing in 2011. He is also an Associate Editor for the IEEE GEOSCIENCE AND REMOTE SENSING MAGAZINE, and was a member of the Editorial Board of the IEEE GEOSCIENCE AND REMOTE SENSING NEWSLETTER from 2011 to 2012, and a member of the Steering Committee of the IEEE JOURNAL OF SELECTED TOPICS IN APPLIED EARTH OBSERVATIONS AND REMOTE SENSING in 2012. He served as the Director of Education Activities for the IEEE Geoscience and Remote Sensing Society in 2011–2012, and is currently the President of the Spanish Chapter of the IEEE GRSS since November 2012. He is currently the Editor-in-Chief of the IEEE TRANSACTIONS ON GEOSCIENCE AND REMOTE SENSING JOURNAL since January 2013. He received the recognition of Best Reviewers of the IEEE GEOSCIENCE AND REMOTE SENSING LETTERS in 2009 and the recognition of Best Reviewers of the IEEE TRANSACTIONS ON GEOSCIENCE AND REMOTE SENSING in 2010, a journal for which he has served as Associate Editor from 2007 to 2012.

Yanfei Zhong (M'11–SM'15) received the B.S. degree in information engineering and the Ph.D. degree in photogrammetry and remote sensing from Wuhan University, China, in 2002 and 2007, respectively

He has been with the State Key Laboratory of Information Engineering in Surveying, Mapping and Remote Sensing, Wuhan University, since 2007 and is currently a Full Professor. His research interests include multi- and hyperspectral remote sensing data processing, high-resolution image processing and scene analysis, and computational intelligence.

Dr. Zhong received the National Excellent Doctoral Dissertation Award of China and New Century Excellent Talents in University of China. He was also a Referee of more than 30 international journals. He is serving as an Associate Editor of *the International Journal of Remote Sensing*, and IEEE JOURNAL OF SELECTED TOPICS IN APPLIED EARTH OBSERVATIONS AND REMOTE SENSING. He has published more than 100 research papers, including more than 45 peer-reviewed articles in international journals such as IEEE TRANSACTIONS ON GEOSCIENCE AND REMOTE SENSING, IEEE TRANSACTIONS ON SYSTEMS, MAN, AND CYBERNETICS PART B, IEEE JOURNAL OF SELECTED TOPICS IN SIGNAL PROCESSING AND PATTERN RECOGNITION.

Huan Xie received the B.S. degree in surveying engineering and the M.S. and Ph.D. degrees in cartography and geoinformation from Tongji University, Shanghai, China, in 2003, 2006, and 2009, respectively.

From 2007 to 2008, she was with the Institute of Photogrammetry and GeoInformation, Leibniz Universität Hannover, Germany, funded by China Scholarship Council, as a Visiting Scholar. Since June 2009, she has been with the College of Surveying and Geoinformatics, Tongji University, where she is currently an Associate Professor and teaches courses related to GIS and remote sensing. Her research interests include hyperspectral remote sensing and polar remote sensing.

Liangpei Zhang (M'06–SM'08) received the B.S. degree in physics from Hunan Normal University, Changsha, China, in 1982, the M.S. degree in optics from the Xi'an Institute of Optics and Precision Mechanics, Chinese Academy of Sciences, Xi'an, China, in 1988, and the Ph.D. degree in photogrammetry and remote sensing from Wuhan University, Wuhan, China, in 1998.

He is currently the Head of the Remote Sensing Division, State Key Laboratory of Information Engineering in Surveying, Mapping, and Remote Sensing (LIESMARS), Wuhan University. He is also a "Chang-Jiang Scholar" Chair Professor appointed by the Ministry of Education of China. He is currently a Principal Scientist for the China State Key Basic Research Project (2011–2016) appointed by the Ministry of National Science and Technology of China to lead the remote sensing program in China. He has more than 500 research papers and five books. He is the holder of 15 patents. His research interests include hyperspectral remote sensing, high-resolution remote sensing, image processing, and artificial intelligence.

Dr. Zhang is the Founding Chair of IEEE Geoscience and Remote Sensing Society (GRSS) Wuhan Chapter. He received the best reviewer awards from IEEE GRSS for his service to IEEE Journal of Selected Topics in Earth Observations and Applied Remote Sensing in 2012 and IEEE Geoscience and Remote Sensing Letters in 2014. He was the General Chair for the 4th IEEE GRSS Workshop on Hyperspectral Image and Signal Processing: Evolution in Remote Sensing and the guest editor of JSTARS. His research teams won the top three prizes of the IEEE GRSS 2014 Data Fusion Contest, and his students have been selected as the winners or finalists of the IEEE International Geoscience and Remote Sensing Symposium student paper contest in recent years. He is a Fellow of the Institution of Engineering and Technology, executive member (board of governor) of the China National Committee of International Geosphere–Biosphere Programme, executive member of the China Society of Image and Graphics, etc. He received the 2010 Best Paper Boeing Award and the 2013 Best Paper ERDAS Award from the American Society of Photogrammetry and Remote Sensing (ASPRS). He regularly serves as the Co-Chair of the series SPIE conferences on multispectral image processing and pattern recognition, conference on Asia remote sensing, and many other conferences. He edits several conference proceedings, issues, and geoinformatics symposiums. He also serves as an Associate Editor of the *International Journal of Ambient Computing and Intelligence*, the *International Journal of Image and Graphics*, the *International Journal of Digital Multimedia Broadcasting*, the *Journal of Geo-Spatial Information Science*, and the *Journal of Remote Sensing*, and the Guest Editor of the *Journal of Applied Remote Sensing* and the *Journal of sensors*. Heis currently serving as an Associate Editor of the IEEE TRANSACTIONS ON GEOSCIENCE AND REMOTE SENSING.